

Microstructure Investigation, Hot Tensile and Hot Corrosion of IN600 to Nimonic 75 heterogeneous Connection in Spot Welding

Sepehr Poor Morad Kaleybar^a, Hami Molla Safari^a, Zahra Sadat Seyed Raofi^b, Yazdan Shajari^c,
Hamid Bakhityari^{c,*}

^a *Materials Engineering and Metallurgy, Khajeh Nasir al-Din Toosi University of Technology, Tehran, Iran*

^b *Faculty of Materials Engineering, Islamic Azad University, Karaj, Iran*

^c *Materials and Energy Research Institute, Faculty of Materials, Karaj, Iran*

Article Info

Article history:

Received Dec 20th, 2020

Revised Feb 19th, 2021

Accepted Mar 4th, 2021

Keyword:

Resistance spot welding

Ni-based superalloy

Inconel 600

Nimonic 75

Hot corrosion

Abstract

Nimonic 75 and Inconel 600 alloys are the Nickel-based superalloys which are used in manufacturing gas turbine components. In the current research, a superalloy Ni-based Nimonic sheet and Inconel 600 were used, joint by resistant spot welded (RSW) machine at currents of 2, 4, and 6 kA, pressure of 5 and 7 bar, and times of 0.6, 0.9 and 1.2. Non-destructive inception methods and light and scanning electron method (SEM) and light optic microscope (LOM) were used to evaluate joints' quality. Shear and micro-hardness test was used to check the mechanical properties of the joint. The findings indicate that the most appropriate welding connection of inhomogeneous points at the current of 4 kA was the holding time 0.9 second and electrode force 7bar. The analysis of microstructure consisted of 3 welding zones which are affected by heat and the base metal. The warm corrosion scanning microscope test results at 600 °C and 800 hours confirmed that the existence of a chromium oxide layer on the surface of the superalloy, which has the main role in protecting the piece in the output temperature.

1. Introduction

Nowadays, industrial designers need lots of more robust and more corrosion-resistant materials [1, 2]. Among all engineering materials, aluminum alloys and composites are mostly used for anti-erosion and lightweight structures [3-4]. Development of many technologies such as gas turbines, high-pressure hydrogen tanks, and wind turbines, require more efficient materials that can abide significant tensions during longer life cycle [3-5]. Superalloys are one of the limited materials used at higher temperatures and have been developed for use in the hottest parts of a gas turbine [6, 7]. Superalloys are materials that can work at temperatures more than 538 °C and preserve their firmness up to 85% of the melting point temperature. Generally, Superalloys are nickel-based and cobalt-based alloys ordinarily used at temperatures higher than 540 °C. Iron-nickel base superalloys, such as IN-718 alloy, are developed from stainless steel technology and are commonly used. The properties of superalloys can be controlled by adjusting the chemical composition and process (including heat treatment) and obtain excellent mechanical strength in the finished product. To select superalloys to use in the above applications, it is necessary to consider technical properties like ductility, strength, creep strength, fatigue strength and surface stability [6]. In average, half of the weight of a gas turbine is made by superalloys [7]. The two main groups of iron-nickel alloys in which the content of nickel is higher than the amount of iron are Incoloy 706 and Inconel 718 [8]. Inconel is a commercial brand from the group of nickel austenitic base coatings used in very high temperatures. The second element in terms of the percentage of chemical composition is chromium, which changes the covering properties [9, 10]. This alloy is from the nickel-chromium solid solution family and is generally used for high-temperature applications [11].

Nickel-based alloys consist of about 50% nickel and contain remarkable amounts of chromium, cobalt, and refractory metals, but either has less or no iron. They may contain aluminium or titanium. Generally, the local melting temperature

* Corresponding author: h.bakhtiari@merc.ac.ir

➤ This is an open access article under the CC-BY license (<https://creativecommons.org/licenses/by/4.0/>).

© Authors retain all copyrights.

of cobalt-based superalloys is higher than that of nickel-based superalloys. Nickel alloys have higher corrosion resistance than the austenitic stainless steels used in industries. Nickel alloys are more expensive than stainless steels because of the higher worth of the element nickel than iron, but they also can change to alloy with more elements such as molybdenum than stainless steel [12].

Generally, nickel-based alloys are divided into two groups: corrosion resistance alloy (CRA) in wet environments or dense aqueous systems, and high-temperature alloys (HTA) are used in systems disposing to gaseous or dry corrosion. The fundamental alloying element in nickel alloys is chromium, which protects the material in passivation conditions by forming a chromium oxide (Cr_2O_3) film on the material surface. The formation of a chromium oxide layer protects the part both in aqueous environments and at high temperatures. Two elements that are added to nickel alloys to increase corrosion resistance are molybdenum and tungsten. These elements effectively increase the corrosion resistance of the alloy in acidic environments [13].

Nymonic alloy (UNS 475 N06075/ W.Nr. 2.4951 & 2.463) contains 20/80 nickel-chrome alloy and is controlled by adding titanium and carbon. This alloy's most common use is in the form of a sheet which was first used in 1940 in gas turbine because of its high-temperature resistance and oxidation resistance [13].

Extensive bonding methods used in all superalloys include fusion welding, solid-state welding and hard soldering. The fundamental method of joining superalloys is fusion welding. The welding method of superalloys depends on its strength mechanism for working at high temperatures.

This mechanism can be solid solution strengthening or secondary phase deposition. Melting welding makes a metallurgical bond with a cast structure and grain size and different properties among parts. Also, most of the connections and repairs in parts used at high temperatures like gas turbine engine components, are done by welding, so the weldability of nickel-based superalloys is very important [11]. Spot welding is widely used in shipbuilding, car, aircraft, and turbine industries because of its high speed and ease of usage and automation capability.

As one of the most used types of resistance welding, Spot welding is ordinarily used to connect lip-to-lip sheets, wire to sheet, or wire to wire. Cobalt-based superalloys containing chromium have good corrosion and oxidation resistance, and their welding capability and thermal fatigue resistance are more than nickel-based alloys. In spot welding, the point of the two ending part of considered parts is placed on each other and are kept between the two electrodes. Then, by current flowing through the electrodes and the metals' resistance, the required heat is caught, and at the compressive efficiency that the electrodes applied to the metal, the stations melt, and a weld nugget is created [14, 15].

In this research, the influence of different resistance welding parameters of points similar to Inconel 600 and Nymonic 75 alloys, which are nickel-based superalloys and are used in the turbine and aerospace industries, was analyzed.

2. Research Method

In this research, 75 nickel Nymonic base alloy sheet with dimensions of 125×30 mm and a thickness of 1.5 mm and Inconel 600 with the same dimensions and thickness of 0.8 mm were used. To achieve a proper connection and without external interference, samples were washed with acetone after cutting with a guillotine. To connect the two sheets, the point resistance welding process was used by the IBEROBOT machine (80 PTR) manufactured by the Swedish company. Current intensities of 2, 4 and 6 kA applied force 5 and 7 times and welding time (Per) 30, 45 and 60, equivalent to 0.6, 0.9 and 1.2 seconds, were used.

Totally 18 samples were obtained. The electrode pressure was selected as 7 times as the optimal electrode pressure. The effect of flow and welding time on the samples' mechanical properties and high-temperature strength was investigated; therefore, 9 samples were obtained for microscopic tests and mechanical properties that were coded. EN 970 [16] standard test was used to check the samples visually. Preparation (cutting and polishing) of samples was done based on the standard [17]. To observe the microstructure at the junction, H solution with equal ratios of hydrochloric acid, acetic acid, nitric acid for 10 seconds and IMI-420 light microscope were used. A VEGA / TESCAN Scanning Electron Microscopy (SEM) examined the cross-sectional area of the spot welding joint.

In this research, to investigate the microstructure and analysis of different phases formed at the point of spot welding, the state of return electrons was used and to investigate and study the refractive index of the state of secondary electrons SEM was used. The shear test was performed by Koopa Pazhoohesh TB1-10T dynamic test machine with a strain rate of 10 mm / min and dimensions of 125×30 mm.

After the shear test, the fracture surfaces were examined at the junction of the boiling point by electron microscopy. The Wolpert Instron measured Micro-hardness under a load of 100 g and a loading time of 35 seconds. The hot tensile test was performed by ATM-10T dynamic test machine with a strain rate of 10 mm / min available in the Aviation Industry Organization. The hot tensile test was performed at environment temperature and 600 °C (operating temperature of the superalloy) to compare the boiling point sample, creating the best properties.

After installation inside the machine, the shear sample reached the desired temperature by the element furnace and by the end of the test, the welding area was subjected to the mentioned temperature conditions. Samples were cut according to the standard [18]. Due to the part's operating conditions exposed to hot compressed gas; therefore, a controlled atmospheric tube furnace was used to perform the hot corrosion test. After finishing the hot corrosion process, the samples were taken out of the furnace based on the schedule and were metallographic to investigate the microstructure. Also, to investigate the degree of part destruction quantitatively, before and after the test, the samples' weight was measured with a digital scale with an accuracy of one-tenth of a thousandth (4 digits) of the AND model. Corrosion levels at the weld site were examined by electron microscopy after the hot corrosion test.

3. Results and discussion

In the parts of superalloys created by the welding spot machine (samples 4 to 6 - group 2), no welding defects such as cracks, impurities and incomplete melting were noticed, and therefore their appearance is confirmed. The visual inspection results confirmed the dimensional accuracy and proportion of the joint, during and after welding. The results of the visual inspection test are indicated in Table (1). The Samples welded at 4 kA were evaluated with penetrant fluids. Only the samples which were welded with a current of 4 kA and a welding time of 0.9 and 1.2 seconds had no welding cavity defects. Figure (1) shows the weld cavity defect identified in samples 7, 8 and 9.

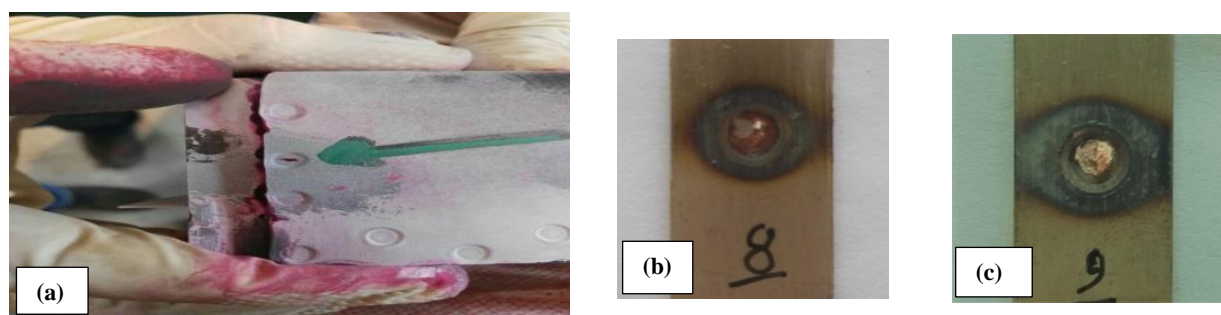


Figure 1. The results of the penetrant fluid test indicating the defect of the cavity in the weld (a) the joint area, (b) and (c) big grains.

Table 1. Specifications and results of eye inspection test. Samples were investigated for dimensions and appearance before, during and after welding.

Connection type	(Lap Joint)
(mm) Connection / Dimensions	horizontal30×30
Preheating temperature	room temperature
Heat treatment after welding	Negative
Type of samples / dimensions	Sheet / 30 × 125 mm
Sample thickness	5/ 1 to 0.8 mm
Admission range	AWS D17.2
result	accepted

The joint area between the two nickel-based superalloy pieces of Figure 1 (2-a), shown as a continuous line, represents that the metallurgical joint is not fully connected in that area. The considered electric current intensity for this sample is 2 kA, which has been applied at different welding times of 0.6, 0.9 and 1.2 seconds, respectively. The microstructure formed around the joint line between two nickel-based superalloys in sample No. 3. Figure (2-b), is in the form of big grains. The grain size decreases with a slight slope as it moves away from the connection line. The deformation of the grains in this path shows the low effect of electric current on the joint. Because of its thickness and high amount of nickel and chromium, Nimonic 75 alloy transfers heat less than Inconel 600.

In 4th sample, by increasing the intensity of electric current up to 4 kA, an attempt was made to improve the connection; but the result was a hole formation based on Figure (3-a) in the center of the connection of two pieces due to the connection.

The reason for the formation of this drop-shaped hole can be related to the two main factors of variable parameters of the spot welding process (time and flow) [19]. Incomplete melting and penetration in spot welding is because of the thickness and type of base material [20].

The second reason, which is the low freezing speed in the joint area, can be considered another factor in causing such defects in spot welding [21]. More attention to the connection area and the joint line between the two pieces can be seen that the hole is inclined towards the Inconel 600 alloy, which is 75 times thicker than the Nymonic alloy due to its less thickness. On the other hand, Inconel alloy piece has less corrosion resistance than Nimonic alloy. This feature can be considered by comparing the components' two surfaces, which was darkened by reaction with the H solution. The inconel alloy surface is darker than nymonic, which shows its low corrosion resistance than nymonic alloy [22]. According to Figure (3-b), the welding area of the 4th sample is shown. This area consists of three main parts. The darkness of these areas is because of the low corrosion resistance of the rejected alloy elements compared to the nickel-rich areas [23]. By increasing the welding time to 0.9 seconds with the same intensity of the previous electric current (4 kA), a connection is formed in the 5th sample. According to Figure (4-a), unlike sample 4, there is no trace of the hole in the joint.

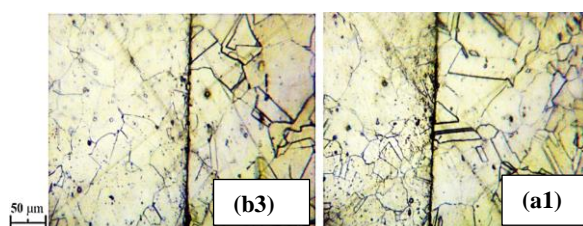


Figure 2. Optical microscope image of a spot welding sample with code (a1) and (b3)

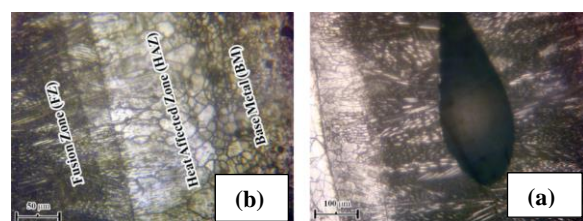


Figure 3. Light microscope image of a boiling point sample with code 4, (a) low magnification, and (b) higher magnification indicating triple welding regions.

This experiment indicates that the destructive reason is the reduction of welding time in sample 4 as predicted (in sample analysis 4). Besides, observing Figure (4-b) shows that the HAZ area in this sample is much smaller than the sample 4, which promises to decrease micro-cracks in that area because the HAZ area is the most susceptible area for micro-crack growth. In the melting zone or FZ of sample 5, which is fully shaped, two different cell-dendritic microstructure types are noticed. Their growth is alternate because of the low amount of copper in their chemical composition. Observing the boiling zone of sample 6 in Figure (4-c), it is clear that its HAZ area has a meaningful increase compared to sample 5, which can be attributed to the heat-affected by the boiling zone on that region.

Like the previous samples in which the HAZ region is shaped, in Figure (4-d), sample 6, after quick freezing in the melted zone (FZ), the grains are transformed from a thin sharp needle to a thicker needle, which is then passed through from the HAZ area are geometrically angled, indicating the effect of the temperature cycle on the boiling zone.

Figure (5) shows the SEM image of the welding area of the optimal welded sample (code 5). Point analysis of different welding areas is also listed in Table (2). In ta research conducted by Razmpoosh et al. [23], scanning electron microscope images of the fracture surface of destroyed samples from the HAZ region show soft fracture with some sheets. The elemental analysis picture (MAP) of the sample with the highest current intensity and time is shown in Figure (6). The penetration of copper element from the electrode during welding to the samples' surface is evident in this analysis, which will lead to the formation of brittle phases and the emergence of cracks in the HAZ area. In optimizing spot welding parameters, the electrode's lack of copper penetration is also a serious and influential factor in welding quality. Increasing the welding current due to increasing the inlet heat increases the HAZ area and increases the nugget diameter, which leads to an increase in strength in the welding area and results in a failure mode of the nugget exit and rending of the sheet.

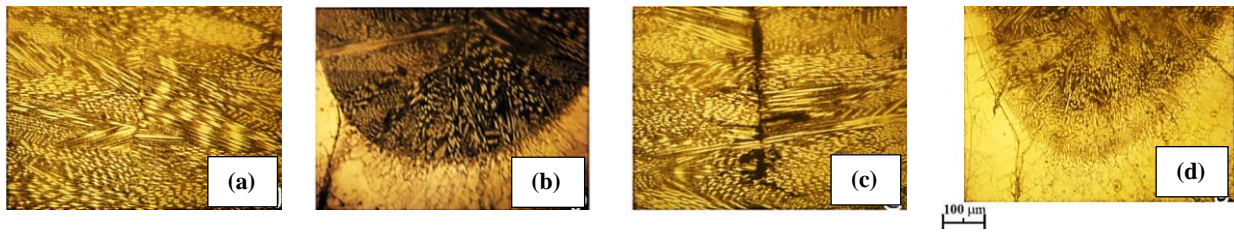


Figure 4. Optical microscope image of the welding area and joint of a spot sample with code 5 (a and b) and code 6 (c and d).

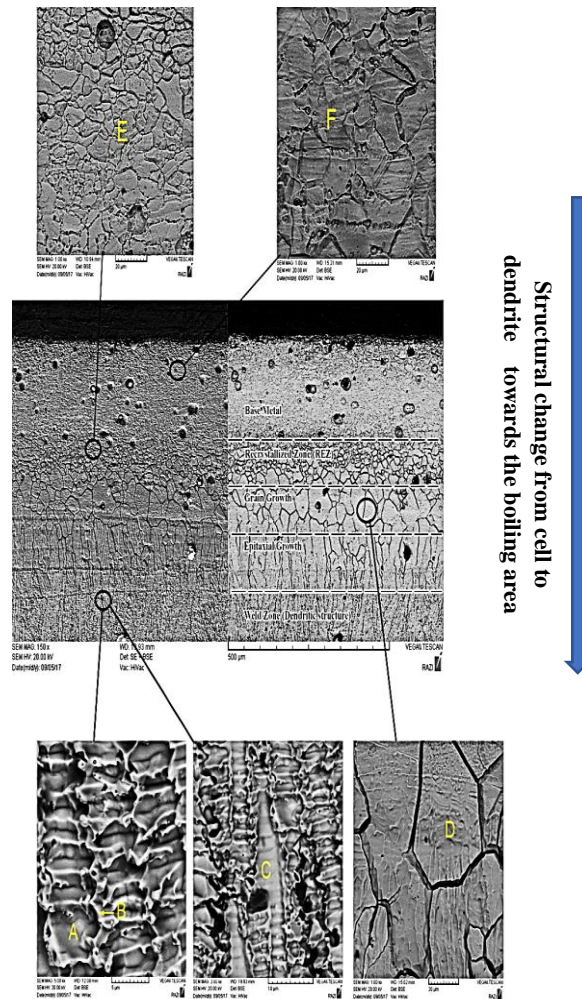


Figure 5. The SEM image in both SE and BSE cases indicates different weld structures across the sample and the change in the cell structure of the base metal to dendrites in the weld area (Latin symbols show different spots of point analysis listed in Table (3)).

In the welded area, the failure mode results in the exit of the nugget and the rupture of the sheet. Microstructural investigations indicated that with increasing flow, grain growth occurs in FZ and HAZ areas. Increasing the welding time shows the same effect. The more significant the stiffness difference between the FZ and HAZ areas, the more likely a nugget exit failure mode. These findings have been mentioned in the research done by Razmpoosh et al. [23]. Thus, the failure mode in sample 1 with the lowest welding current and time is a typical interval with low hardness difference between HAZ and FZ regions. The proximity of the hardness of different areas in the weld makes the preference for the joint interval's failure. The tensile-hot shear test results and the force diagram in terms of displacement are shown in the results of this test in Table (3) and Figure (7), respectively. As the findings show, the raising in temperature has increased the percentage change in length and has reduced the yield force and the maximum. The yield strength and maximum in this test at 600 °C have been reduced by approximately 20% compared to environment temperature.

Table 2. EDS analysis of different areas in Figure (5).

Chemical composition (weight percentage)							symptom
C	Ti	Co	Mn	Fe	Cr	Ni	
0.1	0.88	1.75	1.48	5.07	84.18	96.17	A
63.0	51.0	56.0	01.0	98.4	66.19	38.73	B
09.0	-	65.0	53.0	16.5	06.18	20.69	C
08.0	-	42.0	27.0	53.4	47.18	48.75	D
05.0	-	81.0	-	96.3	00.19	11.76	E
1.0	08.0	-	32.0	78.9	40.16	41.73	F

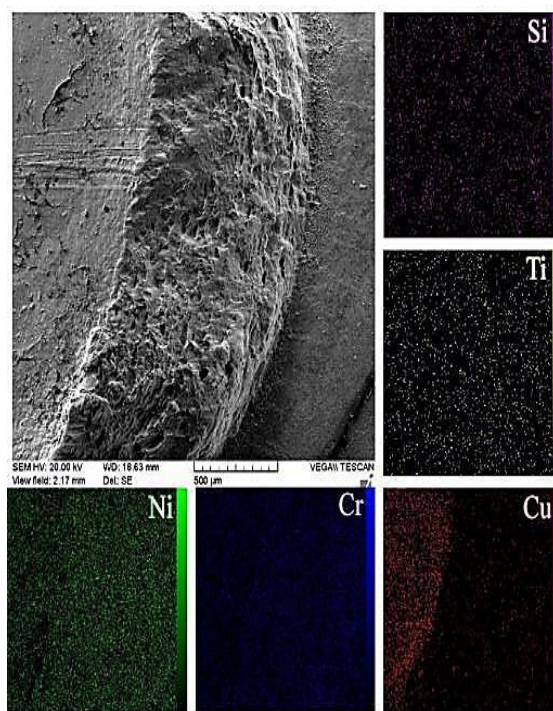


Figure 6. Elemental analysis of MAP from the failure level of sample 8 confirms copper's existence.

With due attention to the failure of both base metal samples and the melting temperature of these superalloys, it can be concluded that the decrease in properties is because of the appearance of dynamic recovery phenomenon in superalloys. Based on Mills theory [24], the failure at environment temperature is because of the concentration of stress around the grain boundaries and the joining of micron cavities at the carbide and ground boundaries, which causes the grains to break.

Table 3. Results of the hot tensile test compared to tensile at room temperature for sample 5

Length change (%)	The highest force (N)	Surrender Force (N)	Test temperature (°C)
5/15	3307	1875	25
17	2799	1482	600

Comparing shear stress at both environments and working temperatures for the boiling point sample shows low yield strength and failure at high temperatures. Figure 8(a) shows two samples after the tensile test at environment temperature and 600 ° C. It should be mentioned that nickel-based superalloys were developed and expanded primarily for service at high temperatures (above 550 ° C) and the tensile strength of these alloys is higher than that of many engineering materials, such as high-alloy steels [6]. The findings of the hot tensile test in this research were consistent with other references [24, 25].

Figure 8(b) shows that the graph of weight changes at different boiling point samples at different times with optimal conditions (code number 5) is indicated.

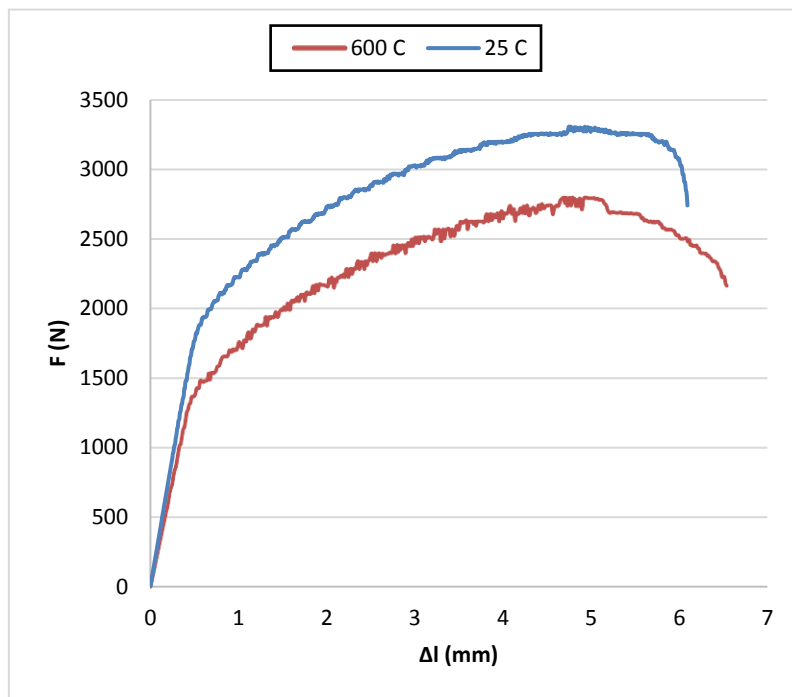


Figure 7. Force diagram to change the length for sample 6 at 25 and 600 ° C

Based on the diagram's numerical findings, it can be noted that the rate of weight gain is increasing up to 500 hours and after that, the rate of change is almost stable up to 800 hours. Weight increasing is because of the formation of oxide layers, especially chromium, on the superalloy and welding area's surface.

In 800 hours weight gain has almost tripled. Based on visual checks and numerical findings, the presence of small and spallation layers of chromium oxides on the superalloy's surface was confirmed.

This research's findings are compared with the previous study conducted in which the nickel base superalloy sample contained 19.5%, 51.6% and 13.7% by weight (respectively) of chromium, nickel, and iron.

This gas superalloy with a composition (volume percentage) of 15% CO / CO₂ -2% H₂O-0.12% H₂S-N₂ was tested at 500 ° C. The most influential element that indicates high resistance to hot corrosion is chromium [26]. This element combines with oxygen to form the Cr₂O₃ phase, preventing further degradation of the base metal. In other words, to improve the properties of hot corrosion resistance, at least 16% by weight of chromium should be present in the initial microstructure of the superalloy.

Figure (9) shows a scanning electron microscope image of a sample with code 5 after 200 and 800 hours of hot corrosion test at 600 ° C with MAP analysis.

After putting the sample in the oxide atmosphere for 200 hours as represented in Figure (9-a), an oxide layer is shaped on the superalloy's surface. Continuing the testing time up to 800 hours figure (9-b), this oxide layer has wholly covered the sample's surface, and edge and, compared to the 200-hour sample, and its thickness has not changed significantly.

Analysis of the atomic distribution of elements in the sample's cross-section showed that the oxide layer is mainly composed of chromium (9-c).

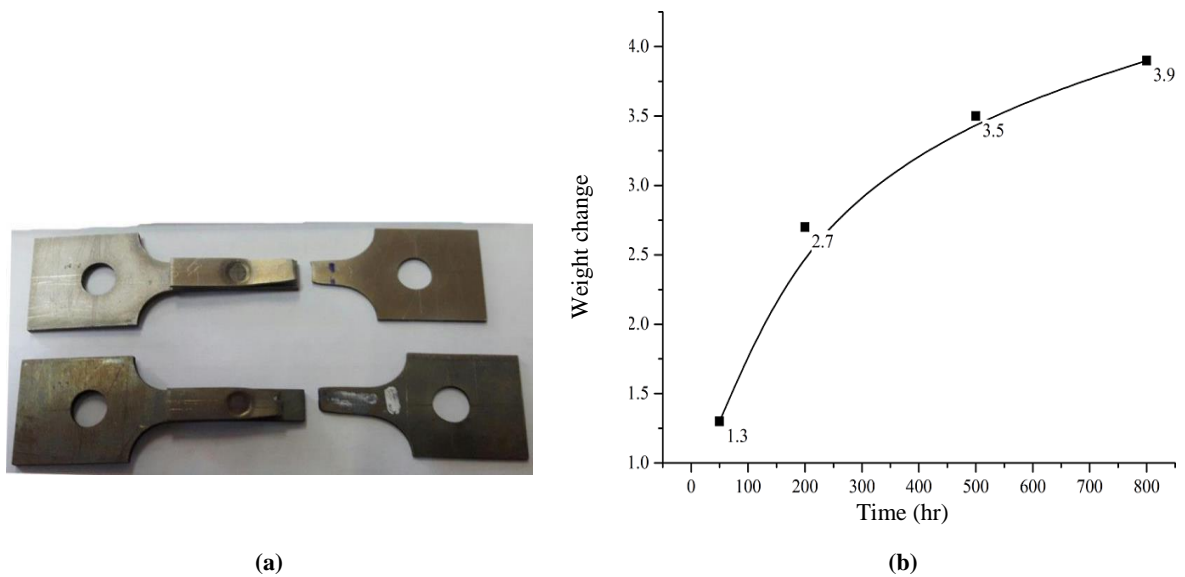


Figure (8): (a) Welded samples after the hot tensile test at room temperature and 600 ° C, (b) weight changing graph in hours for sample No. 5 under hot corrosion test at 600 degree

The oxide layer composition based on point analysis is often Cr₂O₃, which is similar to the oxide layer composition of other sheets in the field of hot corrosion investigation of nickel-based superalloys [26].

In research, investigating the features of nickel-based superalloys at 650 °C under the SC-CO₂ atmosphere, the presence of Cr₂O₃, CrFeO and NiCr₂O₃ oxide phases on the surface of 625 Inconel alloy was confirmed by SEM-MAP test. Therefore, all superalloys used in the construction of turbines have a particular life limitation, after which they should be removed from the turbine assembly and should be installed on the system after repairing and so-called re-peeling.

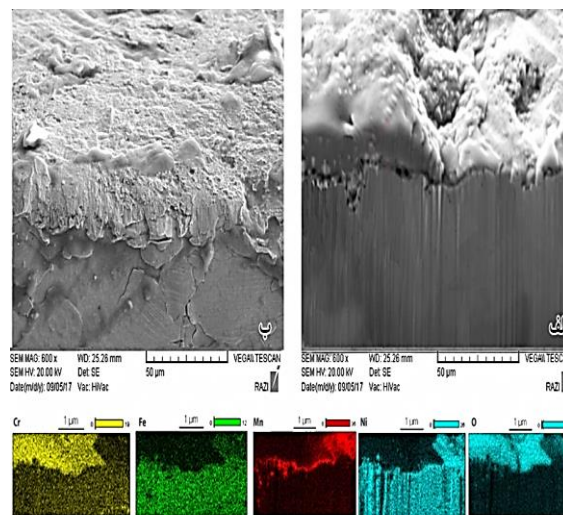


Figure 9. Scanning electron microscope image of the sample edge with code 5 after (a) 200 and (b) 800 hours under hot corrosion test, (c) MAP analysis

4. Conclusions

Based on the research conducted about the non-destructive, the electrode pressure is optimal in the amount of 7 times and has created a desirable connection. The microstructure of Nimonic 75 and Inconel 600 alloys mostly consists of the base phase γ (austenite enriched with nickel), composed of inter-granular compounds and carbides the grain boundary. The joint microstructure includes four parts: the dendritic columnar structure of the weld zone, the fine-grained recrystallization region, the coarse-grained recrystallization region, and the recovered region. The dendritic growth of the weld zone structure is because of the high freezing speed, which grows vertically to the cross-section of the sheet

width. A hole in the welding center was observed for all samples except the part welded with a current of 4 kA and a time of 0.9 seconds.

The SEM test findings indicated that because of the lack of alloying elements such as niobium and molybdenum in the microstructure of superalloys, separation does not happen in the weld zone. Based on the point analysis from different boiling zone areas, carbide phases have accumulated at the grain boundaries, and freezing parameters have caused microstructural morphological changes.

The maximum shear force in the best conditions has reached 645 N, in which the base metal has failed. The maximum hardness relates to the fundamental metal with an amount of approximately 320 Vickers. In the HAZ region, the hardness has decreased to 260 Vickers because of the recrystallization phenomenon. By increasing the welding current up to 4 kA, soft fracture zones with pond morphology appear on the fracture surface, which based on the findings of fracture analysis, these zones are rich in titanium.

Titanium is a ductile and tough element accumulated at the boundary of dendritic grains at higher welding currents. Based on the findings of the MAP analysis, SEM test, the penetration of copper element from the electrode during welding to the samples' surface with a welding current of 6 kA is evident, leading to the shaping of brittle phases and cracks in the HAZ area.

The hot-shear tensile test results represented that at 600 °C the amount of yield force and maximum has reduced by about 20% compared to environment temperature. Due to the failure of both samples of base metal, it can be concluded that the reduction of properties is because of the occurrence of dynamic recrystallization phenomenon in superalloy. The weld zone structure under the hot tensile test has changed from branched-dendritic to quasi-circles with a particle size of 12.5-10 microns.

References

- [1] A. Kazemi, S. Yang. Atomistic Study of the Effect of Magnesium Dopants on the Strength of Nanocrystalline Aluminum. *JOM*. 71 (2019) 1209-14.
- [2] A. Rostamijavanani. Dynamic Buckling of Cylindrical Composite Panels Under Axial Compressions and Lateral External Pressures. *Journal of Failure Analysis and Prevention*. (2020) 1-10.
- [3] A. Rostamijavanani, M. Ebrahimi, S. Jahedi. Thermal Post-buckling Analysis of Laminated Composite Plates Embedded with Shape Memory Alloy Fibers Using Semi-analytical Finite Strip Method. *Journal of Failure Analysis and Prevention*. (2020) 1-12.
- [4] A. Kazemi. Atomistic Study of the Effect of Magnesium Dopants on Nanocrystalline Aluminium. 2019.
- [5] A. Kondori, M. Esmaeilirad, A. Baskin, B. Song, J. Wei, W. Chen, et al. Identifying catalytic active sites of trimolybdenum phosphide (Mo₃P) for electrochemical hydrogen evolution. *Advanced Energy Materials*. 9 (2019) 1900516.
- [6] M. Okazaki. High-temperature strength of Ni-base superalloy coatings. *Science and Technology of Advanced Materials*. 2 (2001) 357-66.
- [7] A. Luna Ramírez, J. Porcayo-Calderon, Z. Mazur, V. Salinas-Bravo, L. Martinez-Gomez. Microstructural changes during high temperature service of a cobalt-based superalloy first stage nozzle. *Advances in Materials Science and Engineering*. 2016 (2016).
- [8] D. Dye, O. Hunziker, R. Reed. Numerical analysis of the weldability of superalloys. *Acta Materialia*. 49 (2001) 683-97.
- [9] J. Dupont, S. Banovic, A. Marder. Microstructural evolution and weldability of dissimilar welds between a super austenitic stainless steel and nickel-based alloys. *Welding Journal*. 82 (2003) 125.
- [10] I. Mrkvica, M. Janoš, P. Sysel. Contribution to milling of materials on Ni base. *Applied Mechanics and Materials*. Trans Tech Publ2012. pp. 2056-9.
- [11] Z.-x. SHI, J.-r. LI, S.-z. LIU, X.-g. WANG, X.-d. YUE. Effect of Ru on stress rupture properties of nickel-based single crystal superalloy at high temperature. *Transactions of Nonferrous Metals Society of China*. 22 (2012) 2106-11.
- [12] A. Volek, R. Singer, R. Buerger, J. Grossmann, Y. Wang. Influence of topologically closed packed phase formation on creep rupture life of directionally solidified nickel-base superalloys. *Metallurgical and Materials Transactions A*. 37 (2006) 405-10.

- [13] S. Zhang, D. Zhao. Aerospace materials handbook. CrC Press2016.
- [14] M. Pouranvari, H. Asgari, S. Mosavizadch, P. Marashi, M. Goodarzi. Effect of weld nugget size on overload failure mode of resistance spot welds. Science and Technology of Welding and Joining. 12 (2007) 217-25.
- [15] J.C. Lippold, S.D. Kiser, J.N. DuPont. Welding metallurgy and weldability of nickel-base alloys. John Wiley & Sons2011.
- [16] L.M. Gammon, R.D. Briggs, J.M. Packard, K.W. Batson, R. Boyer, C.W. Domby. Metallography and microstructures of titanium and its alloys. ASM handbook. 9 (2004) 899-917.
- [17] A. Standard. Standard test methods for elevated temperature tension tests of metallic materials. ASTM International, E21-09. (2009).
- [18] Z. Han, J. Orozco, J. Indacochea, C. Chen. Resistance spot welding: a heat transfer study. Welding journal. 68 (1989) 363s-71s.
- [19] J. Friedel. Internal stresses and fatigue in metals. Ed. GM Raßweiler and WJ Grube, Amsterdam, 1959.
- [20] H.R.R. Ashtiani, R. Zarandooz. Microstructural and mechanical properties of resistance spot weld of Inconel 625 super alloy. The International Journal of Advanced Manufacturing Technology. 84 (2016) 607-19.
- [21] P. Wei, T. Wu. Effects of electrical current on transport processes in resistance spot welding. Science and Technology of Welding and Joining. 15 (2010) 448-56.
- [22] O. Ojo, N. Richards, M. Chaturvedi. Contribution of constitutional liquation of gamma prime precipitate to weld HAZ cracking of cast Inconel 738 superalloy. Scripta Materialia. 50 (2004) 641-6.
- [23] M. Razmpoosh, M. Shamanian, M. Esmailzadeh. The microstructural evolution and mechanical properties of resistance spot welded Fe–31Mn–3Al–3Si TWIP steel. Materials & Design. 67 (2015) 571-6.
- [24] D.W. Tanner. Life assessment of welded INCONEL 718 at high temperature. University of Nottingham2009.
- [25] E. Francis, B. Grant, J.Q. Da Fonseca, P. Phillips, M. Mills, M. Daymond, et al. High-temperature deformation mechanisms in a polycrystalline nickel-base superalloy studied by neutron diffraction and electron microscopy. Acta materialia. 74 (2014) 18-29.
- [26] J.G.R. Sereni. Reference module in materials science and materials engineering. (2016).